SYNCHRONIZED ATTOSECOND PULSES FOR X-RAY SPECTROSCOPY*

G. Penn†, A. Zholents, Lawrence Berkeley National Laboratory, Berkeley, CA, USA

Abstract

Attosecond X-ray pulses are an invaluable probe for the study of electronic and structural changes during chemical reactions. The wide bandwidth of these pulses is comparable to that of the valence electronic states, and is well suited to probing valence electron excitations using core electron transitions. We investigate a method for creating two synchronized, attosecond soft X-ray pulses in a free electron laser, through optical manipulation of electrons located in two distinct intervals of the electron bunch. Each X-ray pulse can have energy of the order of 100 nJ and pulse width of the order of 250 attoseconds. The central frequency of each X-ray pulse can be independently tuned to separate core electron transition frequencies of specific atoms in the molecule. The time delay between the two attosecond pulses is tunable from a few femtoseconds to a few hundred femtoseconds with a precision better than 100 attoseconds.

INTRODUCTION

Chemical bonds evolve on a time scale of femtoseconds [1]. The advent of extreme ultraviolet attosecond pulses produced with the technique of high harmonic generation in a gas (see Ref. [2] and references therein) have opened up the possibility for direct study of these processes. Promising ideas for the generation of intense x-ray attosecond pulses using free electron lasers (FELs) were also proposed (see Ref. [3] and references therein). Building upon a recent scheme for the generation of attosecond x-ray pulses [4], we propose a method to enable a newly proposed technique [5] for the study of valence electronic wave packets using stimulated x-ray Raman spectroscopy. In the proposed experiment, the first attosecond x-ray pulse, with the carrier frequency tuned to a ground state transition of one atom of the molecule, creates an electronic wave packet of valence electrons that is later probed by the second attosecond x-ray pulse tuned to a ground state transition of another atom of the molecule. The atom specificity helps to define where the wave packet of valence electrons is created and where it is probed, which simplifies the analysis of the experiment and aids in understanding the spatial distribution of the valence electron wave packets. Individual measurements done with precise and adjustable time delays between the pulses combine into a motion picture showing the dynamics of changes in chemical bonds.

* This work was supported by the Director, Office of Science, High Energy Physics, U. S. Department of Energy under Contract No.DE-AC02-05CH11231.

† gepenn@lbl.gov

While a single pulse could theoretically be split to serve as both the pump and probe, that would limit the functionality of the experiment described above to probing on the same population of atoms that is being pumped. More general use of this method requires pulses at two different frequencies. In the first part of the paper we describe the basic idea of this scheme and in the second part we provide a numerical example. In this example, two x-ray pulses are produced with $\sim$ 250 attosecond FWHM, individually tuned to the K-edges of oxygen and nitrogen.

SYNCHRONIZED-PULSE SCHEME

In the scheme shown in Fig. 1, we combine two recent ideas, current enhanced self amplified spontaneous emission [6] and echo enabled microbunching [7]. The FEL is divided into three sections. Each start with the electron beam acquiring an energy modulation in a wiggler magnet by interacting with a laser pulse. The undulator parameters are chosen to satisfy the FEL resonance condition $\lambda = \lambda_w(1 + K_w^2/2)/2\gamma^2$, where λ is the laser wavelength, $\gamma = E/mc^2$ and E is the electron bunch energy, λ_w is the undulator period, and the undulator parameter $K_w = eB\lambda_w/(2\pi mc)$; here, B is the peak magnetic field, e and m are the electron charge and mass and c is the speed of light. The corresponding laser wave number and frequency are $q = 2\pi/\lambda$ and $\omega = cq$. Following each wiggler magnet is a magnetic chicane, which introduces dispersion R_{56}. In the last two sections, an undulator magnet follows, with period λ_u and undulator parameter K_u which emits radiation at wavelength λ_x due to the bunching imposed on the beam by the previous manipulations.

The first section begins with a long laser pulse with frequency ω_1 interaction with the electron bunch in the wiggler magnet W1, with period λ_{w1} and undulator parameter K_{w1}. This interaction produces a modest sinusoidal energy modulation of electrons with a normalized amplitude $a_1 = \Delta E_1/\sigma_E$ that is slightly greater than unity, where ΔE_1 is the peak electron energy gain in the wiggler and σ_E is the original rms energy spread in the electron bunch. The pulse is sufficiently long that the entire electron bunch is energy modulated by the same amount, and is insensitive to jitter in the relative timing of the electron bunch and the laser. It is assumed here, and in all other cases where a seed laser interacts with electrons, that the cross section of the laser light in the wiggler is several times larger than transverse rms sizes of the electron bunch, and thus all electrons at the same location along the electron bunch receive equal energy change according to the phase of the laser light at the beginning of the interaction. A chicane C1 with rather large $R_{56}^{(1)}$ follows, which yields a characteris-

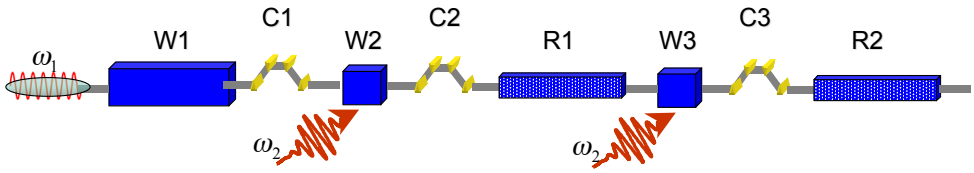

Figure 1: A schematic of the generation of two attosecond x-ray pulses, where W1, W2 and W3 are wiggler magnets, C1, C2 and C3 are magnetic chicanes, R1 and R2 are x-ray undulator radiators, ω_1 is the carrier frequency of the long laser pulse and ω_2 is the carrier frequency of the few-cycle laser pulse.

tic electron distribution in longitudinal phase space which is nearly uniform on long length scales but on short length scales is composed of narrow bands of electrons separated by similarly narrow bands of empty phase space. This is a critical step that prepares the electrons for subsequent microbunching at wavelengths much shorter than λ_1 via transformation of a narrow spacing of energy bands into narrow microbunches along the coordinate axis.

As proposed in Ref. [7], this transformation is achieved by applying a second energy modulation of the electrons in a second wiggler magnet W2, seeded by a laser at frequency ω_2. For our purposes, the normalized amplitude of energy modulation $a_2 = \Delta E_2/\sigma_E$ should be large, of the order of 10–20. This second seed laser prepares the electron bunch for the production of the first of the attosecond pulses, and so we use a few-cycle laser pulse with carrier-envelope phase stabilization (see, for example, Ref. [2]) and a wiggler magnet with only one period, to apply the energy modulation in as short an interval of the electron bunch as possible. The electric field vanishes in the center of the laser pulse (see the insert in Fig. 2).

After the second wiggler, the electron bunch passes the second magnetic chicane C2 whose strength $R_{56}^{(2)}$ is much smaller than $R_{56}^{(1)}$. As a result, we obtain the pattern of current enhancement shown in Fig. 2 with one large central peak and two side peaks [6]. At the same time, the bands of electrons rotate in longitudinal phase space and appear on the coordinate axis as shown in Fig. 3. This indicates an ultra fine microbunching structure of electrons inside the spikes of the peak current. According to Ref. [7], to optimize the microbunching at a small period λ_{x1} corresponding to harmonic number $h_1 = \lambda_2/\lambda_{x1} = |n_1 + q_1/q_2|$ one should choose parameters that satisfy:

$$R_{56}^{(1)} q_1 \frac{a_2\sigma_E}{E} \simeq |n_1| + 0.809\,|n_1|^{1/3}\,, \qquad (1)$$

$$R_{56}^{(2)} = -\frac{R_{56}^{(1)} q_1 - E/\sigma_E}{q_2 n_1 + q_1}. \qquad (2)$$

Here n_1 is a large positive or negative integer number. We note that for a short seed pulse, as above, the harmonic number h_1 does not stricly need to be an integer because of the intrinsic bandwidth. The parameters are carefully chosen to maximize the microbunching only inside the central spike of the peak current (see Fig. 3). Even in the side peaks, the bands in phase space are not fully upright and the microbunching is much weaker.

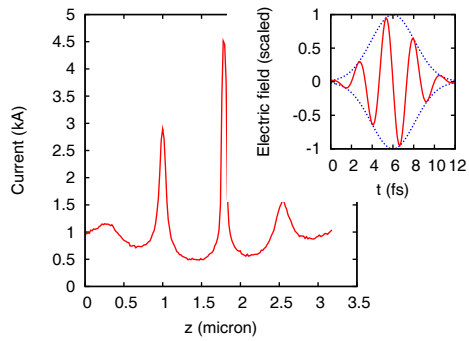

Figure 2: The enhancement in the electron peak current due to interaction with a few-cycle laser pulse with carrier-envelope phase stabilization (see insert).

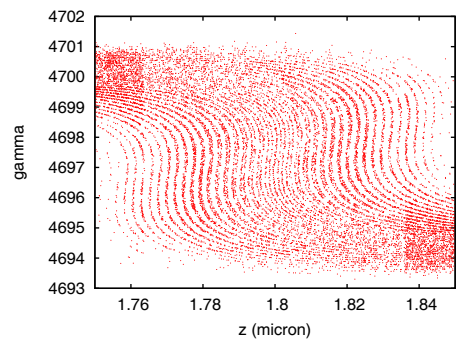

Figure 3: Longitudinal phase space of an interval of the electron bunch after C2, around the central peak.

Following the generation of a narrow current spike, the electron bunch enters the undulator radiator R1 with period λ_{u1} and undulator parameter K_{u1} tuned to the wave length $\lambda_{x1} = \lambda_{u1}(1 + K_{u1}^2/2)/2\gamma^2$. This undulator is moderately short because the central spike in the electron peak current is rather narrow, of the order of $\Delta z_1 = \lambda_2 a_1/2a_2$, and in the case of a large a_2/a_1 slippage between the radiation and spike will limit the useful interaction length. All electrons radiate in R1, but electrons in the central peak (and to some extent the electrons in two side peaks) produce a short pulse of coherent radiation that dominates the radiation of the rest of the electron beam due to the locally enhanced peak current and microbunching.

Having demonstrated how to obtain one attosecond x-ray pulse with the carrier wave length λ_{x1}, a second attosecond

x-ray pulse with carrier wave length λ_{x2} is then generated in the same manner. The beam passes through another wiggler magnet W3, followed by a chicane C3 and radiator R3. The laser pulse for W3 has the same parameters and shape as for W2, which we plan to obtain by splitting one parent laser pulse into two pulses and introducing an adjustable time delay. The wiggler magnet W3 is also the same design as W2. The electrons that overlap the second short pulse while passing through W3 have a distribution which is almost unchanged from W2, except for some additional energy dispersion, and will also aquire a large modulation amplitude a_3. This time we adjust a_3 and $R_{56}^{(3)}$ to optimize the microbunching at a different wavelength λ_{x2} with harmonic number $h_2 = \lambda_2/\lambda_{x2} = |n_2 + q_1/q_2|$ using similar contraints as in Eqs. 1 and 2:

$$a_3 \simeq \frac{|n_2| + 0.809\,|n_2|^{1/3}}{(R_{56}^{(1)} + R_{56}^{(2)})q_1\sigma_E/E}, \tag{3}$$

$$R_{56}^{(3)} = -\frac{(R_{56}^{(1)} + R_{56}^{(2)})q_1 - E/\sigma_E}{q_2 n_2 + q_1}. \tag{4}$$

Note that the cumulative time-of-flight parameter related to the energy bands in phase space is the sum $R_{56}^{(1)}+R_{56}^{(2)}$ from the two chicanes C1 and C2 which the beam has passed through up to this point.

The final undulator radiator R2 is tuned for the FEL resonance at λ_{x2}. Similar to R1, this is a relatively short undulator to match the narrow width of the central current spike. The radiation from this second central spike dominates the output from the rest of the electrons in the bunch, including those electrons in the central peak of the first interval of the electron bunch. The latter do not produce significant coherent radiation in R2 because they have microbunching at λ_{x1}, which is the wrong wave length for this radiator.

NUMERICAL EXAMPLE

For a numerical illustration of the feasibility of the above described scheme we demonstrate generation of two attosecond x-ray pulses with one carrier frequency at the oxygen K-edge and the other carrier frequency at the nitrogen K-edge using the electron beam with the following parameters [8]: 2.4 GeV energy, 1 kA peak current, 0.8 mm-mrad rms slice emittance, 100 keV rms slice energy spread, 200 fs FWHM bunch length.

The amplitude of energy modulation of electrons after interacting with a laser within a wiggler magnet is calculated using the analytic formulas from Ref. [9]. In W1 we have 10 periods with $\lambda_{w1} = 16$ cm and $K_{w1} = 10.4$, the laser frequency is 200 nm. The peak power is chosen to achieve a modulation $a_1 = 3$, and a pulse with 800 fs duration will require 5 μJ of energy.

The chicane C1 has $R_{56}^{(1)} = 17.63$ mm and consists of four bending magnets, each with length $L = 2.5$ m and bending angle $|\theta| = 63.8$ mrad, separated by 0.5 m long drift sections. Here we use rather long magnets in order to have small rms energy spread $\Delta\sigma_E$ induced by quantum fluctuation of synchrotron radiation [10]:

$$\frac{\Delta\sigma_E}{E} = \left(\frac{5}{48\sqrt{3}}\frac{r_e^2}{\alpha}\gamma^5\theta^3\right)^{1/3}\frac{1}{L}, \tag{5}$$

where r_e is the classical electron radius. From Eq. 5, each magnet contributes approximately 0.63 keV in energy spread, which is small compared to the gaps between bands of electrons produced in the first FEL section, estimated to be $E\lambda_1/2R_{56}^{(1)} = 13.6$ keV. The effect of incoherent synchrotron radiation is included from all FEL elements.

For a selective energy modulation of electrons within a few femtosecond long interval of the electron bunch we employ a few-cycle laser pulse with carrier-envelope phase stabilization, a carrier wave length $\lambda_2 = 800$ nm and a pulse length of 3.5 fs (FWHM) for the intensity profile [11]. This pulse is split into two pulses where the first, with energy of 14 μJ, is used in W2 to produce energy modulation $a_2 = 16$, and the second, with energy of 7 μJ, is used in W3 to produce energy modulation $a_3 = 12.4$.

Both wigglers have the same period and undulator parameter, with $\lambda_{w2} = \lambda_{w3} = 25$ cm and $K_{w2} = K_{w3} = 16.7$. The rms energy spread induced by synchrotron radiation in a wiggler magnet with large K is equal to [12]:

$$\frac{\Delta\sigma_E}{E} = \left[4.16\frac{r_e^2}{\alpha}\gamma^2 N\left(\frac{eB}{mc}\right)^2\right]^{1/2}, \tag{6}$$

where N is the number of periods; for W2 and W3 this amounts to 0.32 keV each.

The chicane C2 has $R_{56}^{(2)} = 0.206$ mm and consists of four bending magnets with length $L = 0.6$ m and bending angle $|\theta| = 10.1$ mrad separated by 0.6 m long drift sections. This chicane produces the current spike of Fig. 2 with microbunching at the x-ray wave length $\lambda_{x1} = 2.27$ nm, in accordance with Eqs. 1 and 2 (see Fig. 3). Figure 4 shows the bunching efficiency near the main peak in Fig. 2 calculated using 1D code, dividing the overlap region into slices with width $\Delta z = 3\lambda_2/44$ and defining the slice bunching factor b_k to be:

$$b_k = \frac{1}{n_k}\sum_{j=1}^{n_k} e^{2\pi i z_j/\lambda_{x1}}, \tag{7}$$

where n_k is the number of electrons located within the k^{th} slice. The chicane C3 has $R_{56}^{(3)} = 0.267$ mm, optimizing the microbunching at the x-ray wave length $\lambda_{x2} = 3.03$ nm in the second interval of the electron bunch in accordance with Eq. 4. The energy modulation a_3 from W3 was selected from Eq. 3. The chicane C3 is identical to C2 except for a change in the bending angle $|\theta|$ to 11.6 mrad.

The undulator radiator R1 has 40 periods, periodicity 5 cm and undulator parameter $K_{u1} = 1.41$ tuned for resonance at λ_{x1}. Calculations carried out using GENESIS [13] with initial particle distribution prepared with a 1D code show that in R1, the bunched electrons produce a dominant

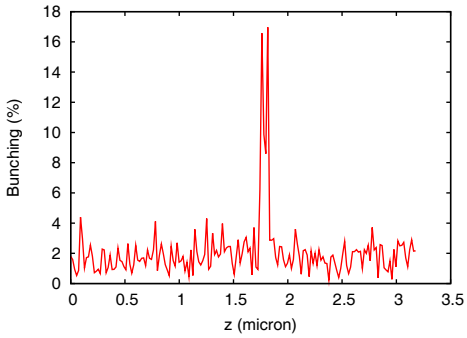

Figure 4: A fragment of the electron bunch showing bunching efficiency. Note, high bunching efficiency is seen only inside the main peak in the electron peak current.

pulse of coherent x-ray radiation, including transverse coherence, with 220 attosecond FWHM. The undulator radiator R2 is similar to R1, but it is adjusted to the undulator parameter $K_{u2} = 1.824$ for the FEL resonance at λ_{x2}. Here, electrons in the second interval of overlap in the electron bunch produce the second pulse of coherent x-ray radiation with 260 attosecond FWHM.

The combined pulses are shown in Fig. 5, with profiles given in terms of both time and spectrum. We note that the electrons from the first interval do not produce large signal in R2 because they are bunched at the wrong wavelength for R2. The time delay between two attosecond pulses is arbitrary and can be easily controlled by synchronizing the seed laser pulses in W2 and W3. In the technique described above, the closest distance between two attosecond x-ray pulses can be as low as $\sim$ 4 fs. This seems to be sufficient for experiments where the minimal interesting time delay between two x-ray pulses is defined by Auger processes of the order of 5–10 fs. The maximum time delay is limited only by the electron bunch length and timing jitter between the electron bunch and the short laser pulses. The x-ray pulse at 544 eV has 8.5 eV FWHM and 102 nJ pulse energy in the spectral peak and the x-ray pulse at 405 eV has 6.6 eV FWHM and 114 nJ pulse energy in the spectral peak. Near this peak there is also a small side peak with 3 nJ total energy.

SUMMARY

Two powerful attosecond x-ray pulses can be produced in an FEL using two different intervals of the electron bunch interacting with ultra-short laser pulses. Here, we demonstrate that by employing the technique of echo-enabled harmonic generation one can actually tune carrier frequencies of these pulses to different values independently from each other. The time delay between these pulses is not affected by jitter in the electron bunch arrival time and can be strictly controlled with high precision as both pulses are synchronized to a single parent laser pulse. All the above listed features are essential for the study of the processes of making or breaking chemical bonds in

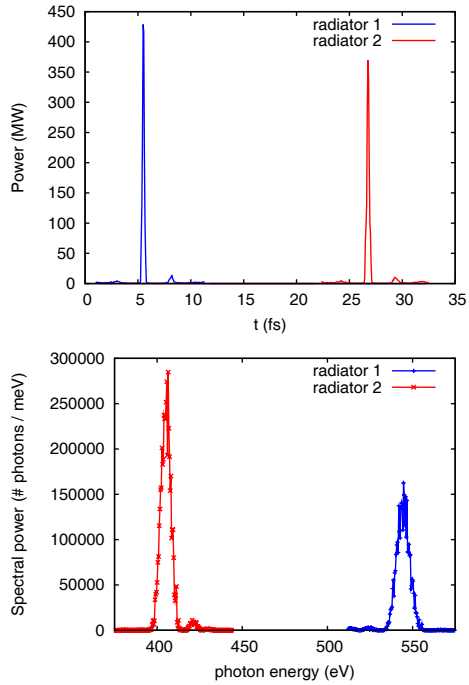

Figure 5: Power (top) and spectrum (bottom) of the two x-ray pulses produced in the undulators R1 and R2. Spectral density is given in units of number of photons per meV.

molecules using x-ray stimulated Raman spectroscopy.

REFERENCES

[1] A.H. Zewail, J. Phys. Chem. A **104** (2000) 5660.

[2] F. Krausz and M. Ivanov, Reviews of Modern Physics **81** (2009) 163.

[3] Y. Ding, Z. Huang, D. Ratner, P. Bucksbaum and H. Merdji, Phys. Rev. ST Accel. Beams **12** (2009) 060703.

[4] D. Xiang, Z. Huang and G. Stupakov, Phys. Rev. ST Accel. Beams **12** (2009) 060701.

[5] I. V. Schweigert and S. Mukamel, Phys. Rev. A **76** (2007) 012504.

[6] A. Zholents, Phys. Rev. ST Accel. Beams **8** (2005) 040701.

[7] G. Stupakov, Phys. Rev. Lett. **102** (2009) 074801.

[8] A.A. Zholents et al., Proc. of Linac conference (Linac08), Victoria, Canada, 2008, p. 501.

[9] A. Zholents and K. Holldack, Proc. Free Electron Laser Conf. 2006, Berlin, (2006).

[10] A.W. Chao and M. Tigner, Handbook of Accelerator Physics and Engineering, World Scientific, Singapore, 2006.

[11] A. L. Cavalieri et al., New J. of Phys **9** (2007) 242.

[12] E. Saldin, E. Schneidmiller and M. Yurkov, Nucl. Instrum. Meth. A **381** (1996) 545.

[13] S. Reiche, Nucl. Instrum. Meth. A **429** (1999) 243.